In-situ fabrication of carbon fibre reinforced polymer composites with embedded piezoelectrics for inspection and energy harvesting applications

Xue Yan,[1] Charles R. P. Courtney,[2] Chris R. Bowen,[2] Nicholas Gathercole,[2] Tao Wen,[3] Yu Jia,[3] Yu Shi [3]

[1] *Science and Technology on Advanced Functional Composites Laboratory, Aerospace Research Institute of Material and Processing Technology, Beijing, 100076, People's Republic of China*

[2] *Materials and Structures Centre, Department of Mechanical Engineering, University of Bath, Bath, BA2 7AY*

[3] *Mechanical Engineering, Thornton Science Park, University of Chester, Chester, CH2 4NU*

E-mail: x_yan@outlook.com

Abstract

Current in situ damage detection of fibre reinforced composites typically use sensors which are attached to the structure. This may make periodic inspection difficult for complex part geometries or in locations which are difficult to reach. To overcome these limitations, we examine the use of piezoelectric materials in the form of macro fibre composites (MFC) that are embedded into carbon fibre reinforced polymer (CFRP) composites. Such a multi-material system can provide an in-situ ability for damage detection, sensing or energy harvesting. In this work, the piezoelectric devices are embedded between the carbon fibre prepreg, and heat treated at elevated temperatures, enabling complete integration of the piezoelectric element into the structure. The impact of processing temperature on the properties of the MFC are assessed, in particular with respect to the Curie temperature of the embedded ferroelectric. The mechanical properties of the CFRP composites are evaluated to assess the impact of the piezoelectric on tensile strength. The performance of the embedded piezoelectric devices to transmit and receive ultrasonic signals are evaluated, along with the potential to harvest power from mechanical strain for self-powered systems. Such an approach provides a route to create multi-functional materials.

Keywords: CFRP, Smart Materials, Sensing, Piezoelectric, Inspection and Energy Harvesting

1. Introduction

There is growing interest in advanced composite materials due to their combination of high strength, high stiffness and low density for applications that require lightweight structures, such as aerospace. In order to improve the functionality of these materials, the potential to combine structural composites with a range of smart material have being considered such as piezoelectric materials, shape memory alloys and optical fibres. Piezoelectric materials embedded in composites are of particular interest since they provide potential for actuation (shape control), the ability to sense strain or impact, vibration control or structural health monitoring. Much of the research to date has simply attached a piezoelectric material or device to the surface of the composite, see for example (Sodano et al., 2004; Song et al., 2010; Eaton et al., 2009; Salamone et al., 2009; Matt and Scalea, 2007; Pullin et al., 2012; Sodano et al., 2006). However, embedding a piezoelectric into the composite structure provides advantages, such as a reduced reliance on external sensors, an ability to operate in complex component geometries or the provision of electrical power to the structure.

As an example of effort to incorporate piezoelectric materials into advanced composites, Geller *et al*. (Geller et al., 2018) examined the process integration of piezoelectric sensors in the form of short fibres within glass-fibre reinforced polymer (GFRP) composites. Weder *et al*. (Weder et al., 2013) considered an automated approach to fabricate intelligent composite components with small piezoelectric fibre components embedded in a GFRP composite using a multi-fibre-injection spray method, with potential for application in structural health monitoring. Bowen *et al*. (Bowen et al., 2014) demonstrated the potential of integrating piezoelectric fibres in a carbon fibre reinforced polymer (CFRP) for actuation or sensing, although the embedding of individual elements and electrode, rather than a discrete device, led to processing challenges. Malakooti *et al*. have presented a novel approach by the growth of piezoelectric ZnO nanowires onto aramid fibres (Malakooti *et al*., 2016).

In order to simplify manufacturing process, the embedding of complete piezoelectric devices have also been considered. Hufenback *et al*. (Hufenbach et al., 2009) examined the creation of dedicated thermoplastic compatible piezoelectric modules for integration into fibre-reinforced composites. Yang *et al*. (Yang et al., 2005), also developed a smart layer module consisting

of polyimide polymer layers and a piezoelectric, where the modular system addressed the challenges of reducing electrical short circuits and improving the ease of electrical connection to the device. The mechanical properties and potential of the system for vibration suppression was examined by embedding in a GFRP composite. Tang *et al*. (Tang et al., 2011) embedded off-the-shelf piezoelectric transducers for structural health monitoring in GFRP for the generation of Lamb waves for damage detection. One reason for embedding in a GFRP material was the electrically insulating nature of the glass fibres, compared to more conductive carbon fibres. The performance of embedded piezoceramic transducers for use as Lamb wave generators was also investigated by Paget *et al*. (Paget et al., 2002), who embedded dense piezoelectrics within a CFRP composite in an effort to improve the efficiency of the process. Konka *et al.* (Konka et al., 2011) embedded piezoelectric transducers manufactured from fibres and embedded macro-fiber composites (MFCs) in a GFRP, with no significant impact on fatigue properties. Finally, the potential for embedding sub-surface piezoelectric sensors into composites was examined by Hu *et al*. (Hu et al., 2007) to identify impact loads and determine impact force history, although the mechanism of embedding the elements was not explained in detail.

The majority of work to date has therefore examined the use of electrically insulating GFRP materials in order to simplify the production process and mitigate electrical short-circuits. Less work has examined the influence of processing temperature on the potential degradation of piezoelectric properties. There is also a potential concern that embedding a piezoelectric transducer in a high stiffness CFRP composite can mechanically clamp the piezoelectric, thereby preventing its use as an embedded transmitter, receiver/sensor or energy harvester. In this paper we have examined the manufacture CFRP materials with embedded piezoelectric transducers with are polarised prior to curing and are able to withstand the processing temperatures. The aim is to achieve minimal degradation of piezoelectric properties so that they can be utilised to both transmit and receive ultrasonic signals for applications related to structural health monitoring, or be used for sensing or energy harvesting. The impact of the piezoelectric on tensile strength are also explored.

2. Method

2.1 Preparation of CFRP with embedded MFC

The multi-functional composites combine CFRP prepreg (CYCOM 977-2-35-12KHTS, from Cytec Engineered Materials Ltd., UK) and a piezolectric MFC (M2814 P2, from the Smart Material Company) in Figure 1. The 2814 of indicates the piezoelectric active area is 28mm by 14mm and the P2 indicates that electrodes are placed on the upper and lower faces with a polarisation direction through the thickness of the device. The high electrical conductivity of the carbon fibres in the CFRP has potential to lead to the formation of an electrical short circuits between the MFC electrodes. As a result, an insulating 'peel-ply' (PP) layer was inserted between the CFRP and MFC layers. Peel ply was selected as it is an isotropic porous fabric which acts as an electrical insulator and prevents the carbon fibres from making direct contact with the piezoelectric; its porous nature also allows the epoxy resin to strongly adhere to the MFC and is compatible with CFRP in terms of processing and does not degrade at the high cure temperate. A variety of composite structures were designed and manufactured in terms of geometry and lay up with a range of dimensions and stacking sequences prepared for electrical testing, mechanical testing, demonstration of use in transmit/receive and energy harvesting in Figure 2-4. The stacking sequence of the composite for intial electrical testing was, $[0^o/90^o/\text{peel-ply}/\ 90^o{}_{MFC}\ /\text{peel-ply}/90^o/0^o]_T$ and is shown in Figure 2. This simple layup was used to examine the impact of curing the composite on the resulting piezoelectric and dielectric properties. The stacking sequence of composite for tensile testing was, $[0^o/90^o/0^o/90^o/0^o/\text{peel-ply}/90^o{}_{MFC}\ /\text{peel-ply}/0^o/90^o/0^o/90^o/0^o]_T$ and is shown in Figure 3. This layup was selected to achieve a sufficent thickness to conform to standard ASTM D3039. The stacking sequence of the composite used for evaluation of ultrasound transmission and reception, shown in Figure 4, was $[0^o/\ 90^o/\text{-}45^o/45^o/\text{peel ply}/\ 90^o{}_{MFC}\ /\ 0^o{}_{MFC}\ /\text{peel ply}/45^o/\text{-}45^o/90^o/\ 0^o]_T$. This was selected since it is a conventional quasi-isotropic layup.

To create the composites, each composite lay-up described above with the embedded MFCs was sealed within a vacuum bag system, where the vacuum ports were placed on the free space of the support to connect with the vacuum pump. It was necessary to keep the bag as flat as possible, without any wrinkles in order to maximise the surface quality of composite plate. All composites were placed into an autoclave at a temperature of 180°C and a pressure of 7 bar (0.7MPa) for 3 hours.

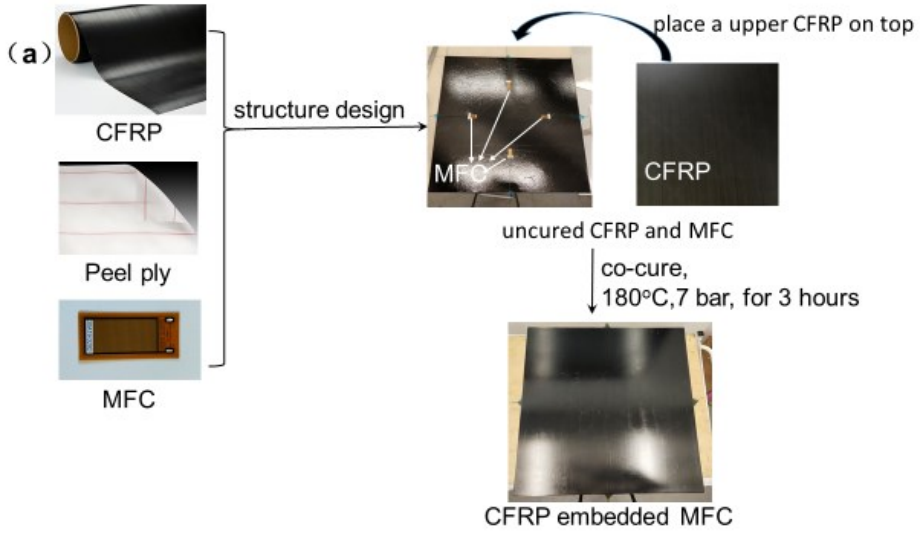

Figure 1. Schematic of processing of CFRP with embedded piezoelectric for a multi-functional composite.

2.2 Electrical characterisation

To assess the impact of processing temperature on the piezoelectric coefficient the MFC was heated to temperatures of 60°C, 100°C, 140°C, 180°C for 1hr in a Delta 9023 thermal chamber; this time was chosen to be representative of the processing time during the high temperature cure. The longitudinal piezoelectric strain coefficient (d_{33}) was then measured using a Berlincourt Piezometer (PM25, Take Control, UK), which is a measure of the charge per unit force in the polarisation direction (thickness direction of P2 MFC device) or a measure of the strain per unit electric field in the polarisation (thickness) direction.

Impedance spectroscopy measurements were carried out using Solatron 1260 and 1296 Dielectric Interface and a two-point probe at frequencies from 1 to 10^6 Hz on the CFRP-MFC composites shown in Figure 2. The modulus of impedance was calculated from,

$$|Z| = \left(Z'^2 + Z''^2\right)^{0.5} \tag{1}$$

where Z' and Z'' are the real and imaginary parts of the impedance. The phase angle (θ) between current and voltage was determined from,

$$\boldsymbol{\theta = \tan^{-1}(Z''/Z')} \tag{2}$$

This was undertaken to examine the influence of (i) the processing on the device capacitance (and therefore permittivity of the piezoelectric) and (ii) the impact of embedding the MFC in a stiff CFRP on the resonant characteristics and this may have an impact on the ability of the piezoelectric to send and receive signals.

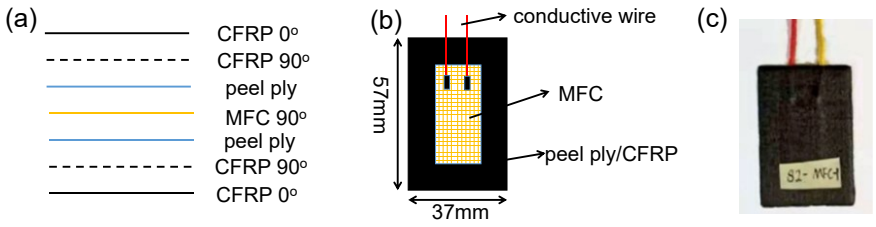

Figure 2. CFRP with embedded MFC for electrical characterisation (a) stacking sequence (b) schematic of test piece (c) image of manufactured CFRP-MFC sample.

2.3 Mechanical test

The tensile test specimen, shown in Figure 3, was cut to dimensions of 250 mm in length and 25 mm in width in accordance with ASTM D3039 standards (ASTM D3039, 2002). The composite was tested in a *INSTRON 5585H* Series Floor Model Testing Systems at a test rate of 2mm/min.

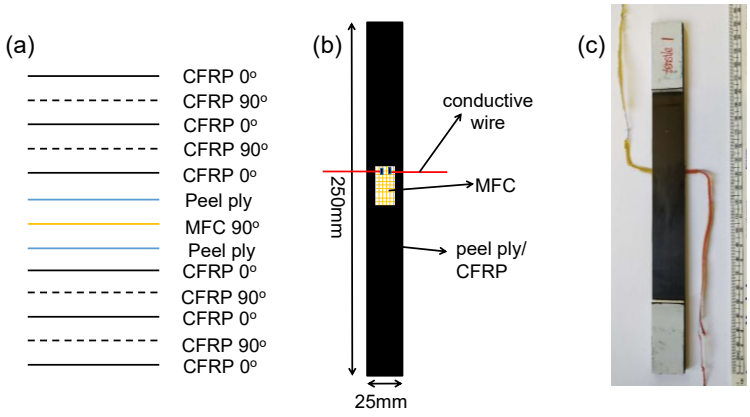

Figure 3. CFRP-MFC for tensile testing (a) stacking sequence, (b) schematic of test piece and dimensions (c) image of manufactured sample.

2.4 Evaluation of performance as an ultrasound transducer

A CFRP plate, shown in figure 8, was prepared with four MFCs in order to demonstrate the performance of the MFCs as embedded ultrasonic transducers. The plate dimensions and MFC placement were selected to ensure good separation of direct transmission between transducers from reflected pulses using the conservative assumptions that the wavelength of the transmitted pulses would be approximately twice the transducer length and that the transducer bandwidth would allow generation of pulses of six cycles or fewer. Hence the MFC devices were located 6L (where L is with MFC length of 28mm) from the composite edge to prevent overlap between direct pulses and pulses initially propagating in the opposite direction, but reflected by the plate edge. The separation was 12L to ensure separation of the directly received signal from any electrical cross talk. The total composite length was therefore 24L.

A combined oscilloscope and arbitrary waveform generator (Handyscope HS3; TiePie Engineering) was used to generate and receive signals. The transmitting MFC was excited with a single cycle of a 12-V amplitude 75-kHz sine wave. The voltage across the receiving MFC was recorded with a sample frequency of 5 MHz. For each test the signal was averaged over 16 repetitions and a 10^{th}-order 500kHz low-pass Butterworth filter applied to remove high frequency noise. Measurements were taken for transmissions from MFCs A to B and C to D, where the locations are shown in figure 4.

2.5 Energy harvesting

The integrated CFRP-MFC composite was characterised using the experimental test setup shown in Figure 4. The sample used was of the same dimensions and configuration as the mechanical testing, as in figure 3, and clamped at one end to operate in cantilever bending mode. Such a confuguration was used to simply demonstrate the potential of the embedded MFC to generate power from mechanical vibrations subjected to the CFRP material. Sine wave acitivitation was used as the input acceleration to excite the vibration shaker via a function generator (model no. Agilent 33210A) and amplified by a power amplifier (model no. LDS PA100. The accelerometer was powered by DC power supply. The MFC embedded inside of the carbon fibre cantilever transferred the mechanical energy to electrical voltage output, which was measured on an oscilloscope (model no. Agilent DSO-X 2004A).

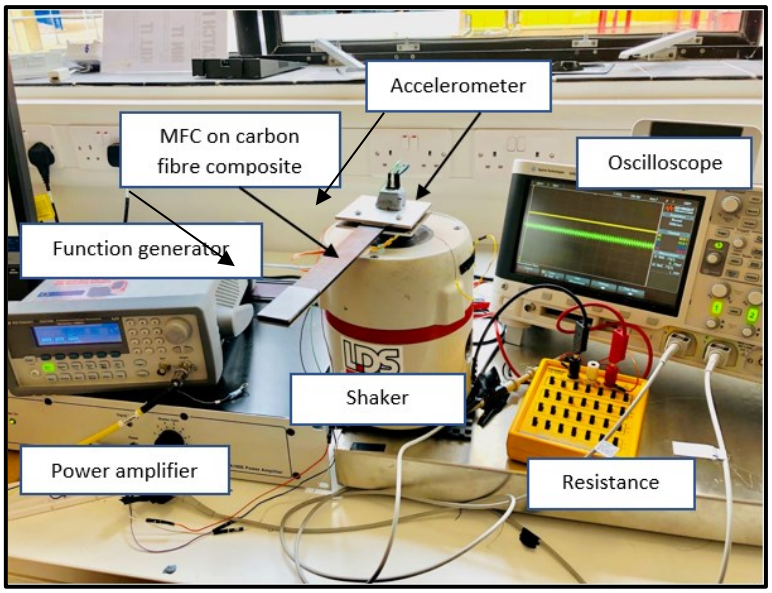

Figure 4. Experimental setup to characterize the energy harvesting response of the CFRP-MFC with a composite geometry in figure 3

3. Results and discussion

3.1 Longitudinal piezoelectric coefficient (d_{33})

The piezoelectric d_{33} coefficients of two identical MFC devices (MFC-1 and MFC-2) with temperature are shown in Figure 5. No significant changes in piezoelectric coefficient are observed with temperature (20 ºC – 180 ºC) for a period of 1hr, indicating that there is potential for co-curing the MFCs with CFRP at temperatures up to the desired composite processing temperature of 180ºC. The data in Figure 6 indicates that the curing of the MFC at processing temperatures of 180 ºC will not significantly affect the piezoelectric d_{33} coefficient. This is due the Curie temperature of the lead zirconate titanate material (PZT-5A) of the MFC being relatively high ($T_c \sim 335$ ºC)[10] and that the remnant polarisation of the material is not reduced during processing. As general rule, the operating temperature of a piezoelectric material is limited to approximately one half of the T_c (in ºC) (Zeng et al., 2015). Therefore, a curing temperature of 180 ºC (~0.53T_c) for 1hr is sufficiently low to avoid depolarisation. It is of interest to note that piezoelectric devices based on a lead zirconate titanate of lower Curie temperature (PZT-5H, $T_c \sim 215$ºC)[10] was fully depolarised ($d_{33} \sim 0$ pC/N) after being subjected to curing temperature of 180 ºC (~0.84T_c) for the same time period.

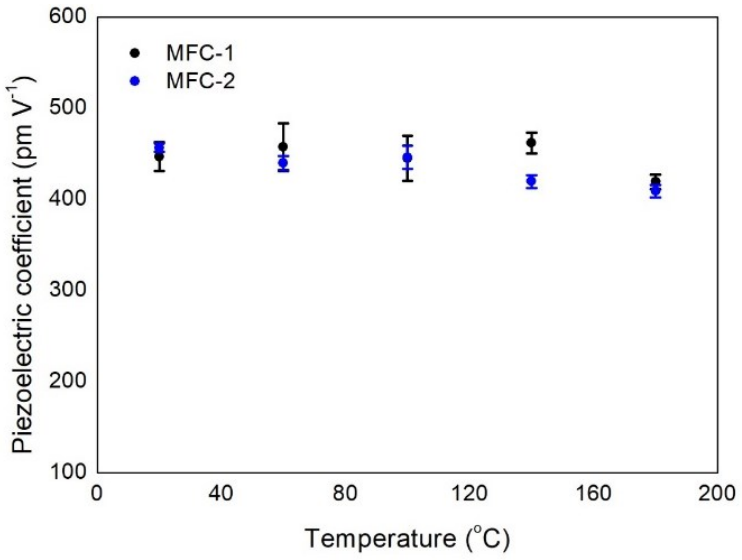

Figure 5. Longitudinal piezoelectric coefficient (d_{33}) of MFC with temperature.

3.2 Frequency dependent impedance and phase angle

The frequency dependent modulus of impedance, from Equation 1, and phase angle, from Equation 2, of the manufactured composites are shown in Figure 6(a) and Figure 6(b), respectively. Data is shown for an MFC that was maintained at room temperature (MFC-20ºC), an MFC that was placed in the autoclave during processing (MFC-180ºC) and the MFC embedded in CFRP and co-curing at 180ºC.

The impedance in Figure 6(a) is frequency dependent and decreases with increasing frequency. This is a result of the piezoelectric material acting as an electrical insulator (dielectric), since the impedance ($|Z|$) of a capacitor follows $|Z|^{-1} \propto \omega C$; where ω is the angular frequency and C is capacitance. This insulating response leads to an almost linear dependency of impedance with frequency in Figure 6(a). At higher frequencies (50 kHz~100 kHz), the impedance of the MFCs which are not embedded in the CFRP are free to vibrate (MFC-20ºC and MFC-180ºC) as a result of a piezoelectric resonance; a clear resonance and anti-resonance which is typical is a piezoelectric element is observed in the inset of Figure 6(a). The fact that the resonance response in not effected by being subjected to a temperature of 180ºC further indicates that the piezoelectric properties (capacitance/permittivity and electro-mechanical response) is not significantly degraded by the application of elevated temperatures and is in agreement with the d_{33} coefficient measurements in Figure 5.

The impedance of the CFRP with an embedded MFC has a similar impedance to MFC-20ºC and MFC-180ºC at low frequencies ($<10^4$Hz) but there is no observable electro-mechanical resonance. This is likely to be due to mechanical clamping of the resonance due to the surrounding high stiffness CFRP material. This overall capacitive response of the three MFCs can also be observed in Figure 6(b), where the phase angle approaches $\theta \sim -90°$, since the ac current lags the ac voltage by 90° in a perfect capacitor.

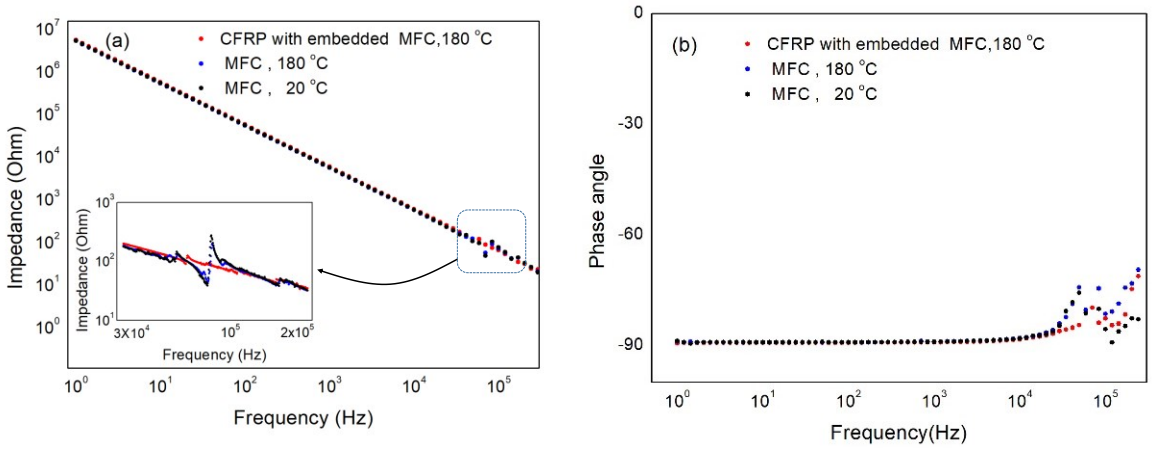

Figure 6. (a) Modulus of impedance $|Z|$of MFC at 20ºC, subjected to 180ºC and CFRP with embedded MFC formed at 180ºC (b) phase angle of MFC at 20ºC, subjected to 180ºC and CFRP with embedded MFC formed at 180ºC.

3.3 Mechanical testing

3.3.1 Tensile testing

A standard CFRP tensile test was undertaken for both samples for CFRP with embedded MFCs as well as CFRP without MFC as a control. The micro-strain dependent load, and failure mode are shown in Figure 7 (a) and Figure 7(b). For both CFRP samples (with and without an MFC) the load increases with increasing strain until the sample fails. The tensile stress at the maximum load of the CFRP with an embedded MFC was 836.5MPa, 7% lower than CFRP without MFC, whose tensile stress at maximum load was 907.1 MPa. The failure mode is shown in Figure 8(b), where the CFRP with embedded MFC fails in the middle section of the test piece, near the location of the MFC; the failure code is XGM by Standard ASTMD3039, where the first character indicates explosive (X) failure, the second character indicates that failure was in the gage (G), and the third character indicates multiple area (M) failure. The CFRP without an MFC failed near the tab, where the failure code is LAT, which indicated a lateral (L) failure, which is angled (A), and located at the top (T) of the sample. This indicates the MFC is a potential origin of failure, due to stress concentrations associated with a stiffness mismatch of the CFRP and MFC. This is agreement with Tang *et al*. who examined failure in tensile fatigue for embedded piezoelectric elements in GFRP and Konka *et al.* who showed stress concentrations near the embedded MFC in a GFRP, but small reduction of strength of 3-6%.

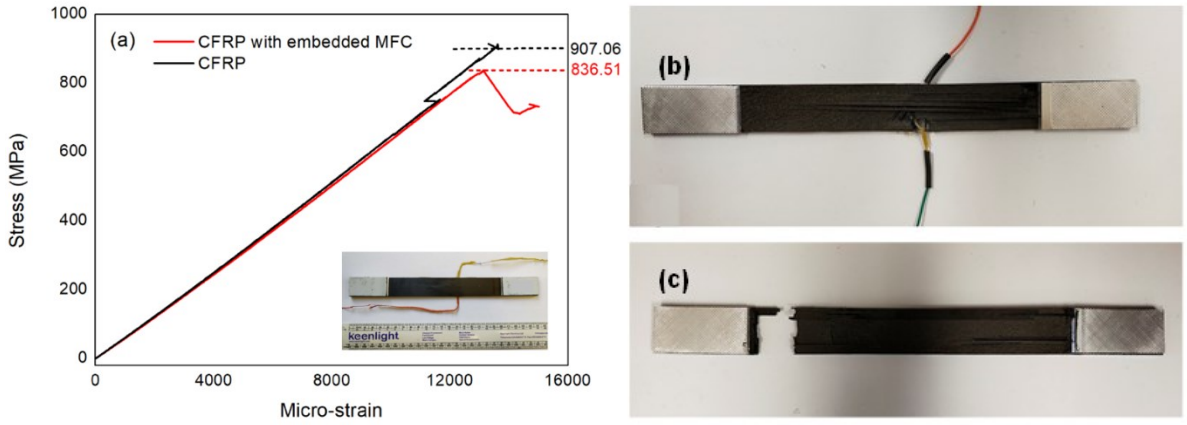

Figure 7. (a) Measured stress-strain curve of CFRP with embedded MFC and without MFC, (b) failure mode of CFRP with embedded MFC, (c) failure mode of CFRP without MFC.

3.4 Evaluation of performance as an ultrasound transducer

Figure 9 shows the resulting signals of the transmission of ultrasound signals from MFC A to B and C to D located in positions shown in Figure 8. Figure 9a shows the voltage applied, V_{in}, to the transmitting MFC. Figure 9b shows the voltage across the receiving MFC, V_{out}. Figure 9c and 9d show the frequency content of the voltage across the transmitting MFC and receiving MFC respectively.

It can be seen that the single cycle of a 12-V amplitude 75-kHz sine wave across the excited MFC is slightly reduced in amplitude. (see Figure 9a) and shifted in the centre frequency to 55 kHz (see Figure 9c). The signal on the receiver MFC, V_{out}, shows a large signal which is simultaneous to the pulse transmission, which is due to electrical cross-talk. This is followed by two clearly separated pulses (one arriving after 59 µs the next after 117 µs) and then the signal degenerates into overlapping pulses due to reflections from the plate boundary. Signals from A to B and C to D are plotted in Figure 9b and are almost indistinguishable, indicating reproducibility of the performance. Opposing transducers are separated by 336 mm (12L, see Figure 4) and therefore the first pulse at 59 µs corresponds to a wave with a group velocity of 5700 ms^{-1} and the larger second pulse 117 µs has a group velocity of 2900 ms^{-1}. Figure 9d shows the frequency content of the received pulses in terms of the first arrival pulse (dotted line) and second arrival (dashed line). Both peaks have centre frequencies of 76 kHz. The second to arrive has a higher peak amplitude (94 µVs), but a smaller bandwidth (55 kHz full width at half maximum) than the more heavily damped first arrival (Peak: 58 µVs, bandwidth: 66 kHz). The bandwidths result in slight elongation of the single-cycle pulses, but pulse lengths below 1.5 cycles are possible. This demonstrates that even after co-curing the embedded MFCs are able to transmit and receive ultrasound within a CFRP material or structure. The degree of damping seen in the reduction in resonance, inset Figure 7a, leads to a broadband response, with the potential to transmit pulses as short as 1.5 cycles at 76 kHz over distances of tens of centimetres.

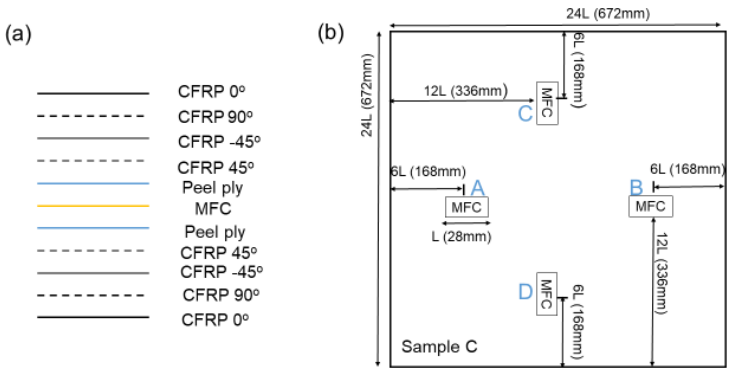

Figure 8. CFRP with embedded MFCs located at A,B,C and D (a) stacking sequence [0°/ 90°/ -45°/45°/peel ply/$90°_{MFC}$ / $0°_{MFC}$ /peel ply/45°/-45°/90°/ 0°]$_T$ (b) schematic of multi-functional composite. L is MFC length, 28mm.

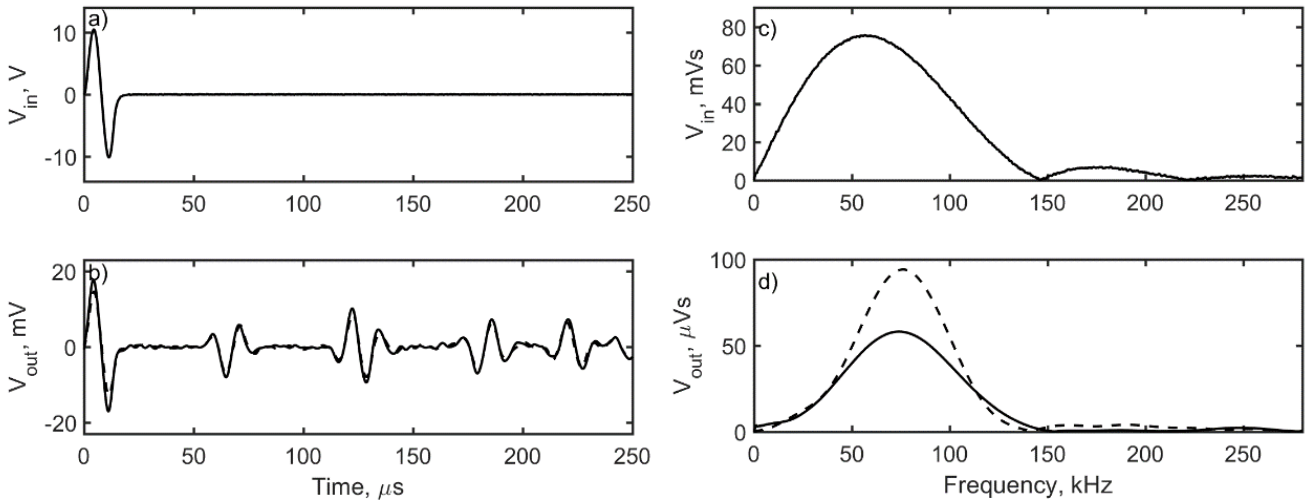

Figure 9. Transmission of ultrasound signals between embedded MFCs. (a) Voltage across transmitting MFC. (b) Voltage across receiving MFC: results for transmission from A to B (solid line) and C to D (dashed line). (c) Frequency content of voltage across transmitting MFC. (d) Frequency content of received pulses: first arrival pulse (dotted line) and second arrival (dashed line).

3.5 Energy harvesting

The first resonant mode was employed to assess the potential for energy harvesting. The first mode was found through adjusting the activation frequency manually to observe the structure amplitude reaction, which is approximately 39 Hz. To verify the result, the output data collected by sweep frequency activation from 20 Hz to 80 Hz in 2 seconds is simulated by a Fourier transform, and the result is shown in Figure 10a. It can be seen that the first resonant mode is 38.57 Hz. Resistance matching of the electrical load (R_L), with respect to capacitve impedance (ωC), found an optimal load at $R_L = 140$ kΩ for the first resonant mode. This is in good agreement with the theoretical optimal load based on a impedance matching the piezoelectric devices with a quoted capaitance of 30.8nF (*Smart Material Corporation*), streucture resonanct frequency of 38.57Hz; where the condition $\omega R_L C=1$ is satisfied at $R_L = 134$ kΩ. The measured harvested energy under first resonant frequency is shown in Figure 10b. As the input vibration amplitude increased, the output RMS voltage (V_{rms}) increased and associated power; $P = V_{rms}^2/R_{Load}$. When the vibration peak-to-peak acceleration achieved 4.9 g, the output RMS voltage was 1.5 V approximately, which relates to 16 µW.

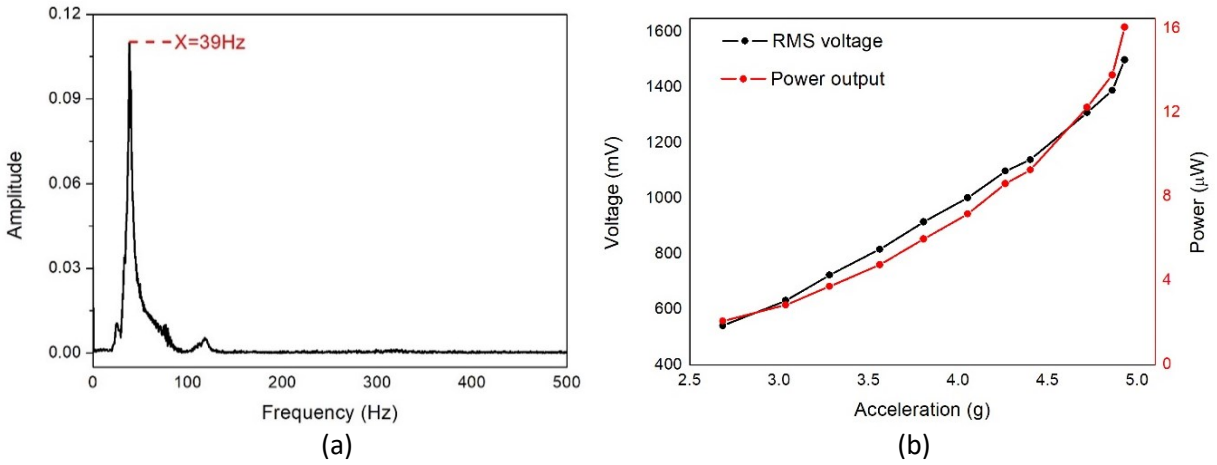

Figure 10. Frequency domain result of CFRP-MFC showing first mode. (b) Experimental voltage output and calculated power results with acceleration when operating at first mode of resonance.

4. Conclusion

This paper has demonstrated the potential for co-manufacturing piezoelectric transducers and advanced structural composites, with potential for multi-functional properties such as ability to provide self-inspection, self-sensing and energy harvesting. Current in situ damage detection of fibre reinforced composites typically often employ methods which require the use of external sensors which must be physically attached to the structure. This may make periodic inspection difficult, in particular for complex part geometries or in locations which are difficult to reach. To overcome these limitations, this work has demonstrated how the use of piezoelectric materials in the form of macro fibre composites (MFC) that are embedded into carbon fibre reinforced polymer (CFRP) composites during the curing process. Such a multi-material configuration is of interest since it can provide an in-situ ability to sense damage or harvest mechanical energy.

In this work, commercial MFC devices were embedded between the carbon fibre prepreg, and heat treated with the CFRP at elevated temperatures, thereby enabling complete integration of the piezoelectric sensing element into the CFRP material and structure. The impact of processing temperature on the properties of the MFC are assessed, such as capacitance and piezoelectric coefficients, in particular with respect to the Curie temperature (T_c) of the embedded ferroelectric. The mechanical properties of the composites are also evaluated to assess the impact of the piezoelectric on tensile strength. The MFCs were shown to be capable of operating as send-receive pairs, transmitting 76-kHz broadband pulses. The ability to send short (1.5 cycle) pulses over tens of centimetres indicates that these embedded devices could be used as transducers for SHM applications with good location accuracy over regions tens of centimetres across. Finally, the potential to also harvest small amounts of power from mechanical strain is also evaluated to examine future potential to create a self-powered system. Such an approach provides a route to create multi-functional materials. It would be of interest to examine the possible influence of residual stresses on the piezoelectric properties. Such residual stresses can originate from the thermal expansion mismatch between the piezoelectric device and the CFRP. There is also scope to provide additional functionality since piezoelectric materials are also pyroelectric with charge generation in response to thermal fluctuation, or to use the change in resonance during curing to also self-monitor curing progression from a change is resonance.

5. Acknowledgments

Dr. Xue Yan acknowledges China Scholarship Council fund.

References

ASTM D3039 (2002) Standard test method for tensile properties of polymer matrix composite materials (West Conshohacken, PA: ASTM International)

Bowen CR, Watson M, Betts DN, et al. (2014) Piezoelectric Fibres Integratedinto Structural Composites. *Ferroelectrics* 466: 14-20.

Eaton M, Pullin R, Holford K, et al. (2009) *Use of Macro Fibre Composite Transducers as Acoustic Emission Sensors*.

Geller S, Tyczynski T, Gude M, et al. (2018) Glass Fiber-Reinforced Polyurethane Composite Structures with Integrated Piezoelectric Sensor Elements and Corresponding Electronics. *Advanced Engineering Materials* 20: 1800447.

Hu N, Fukunaga H, Matsumoto S, et al. (2007) An efficient approach for identifying impact force using embedded piezoelectric sensors. *International Journal of Impact Engineering* 34: 1258-1271.

Hufenbach W, Gude M and Heber T. (2009) Development of novel piezoceramic modules for adaptive thermoplastic composite structures capable for series production. *Sensors and Actuators A: Physical* 156: 22-27.

Konka HP. (2011) Embedded Piezoelectric Fiber Composite Sensors for Applications in Composite Structures.

Matt HM and Scalea FLd. (2007) Macro-fiber composite piezoelectric rosettes for acoustic source location in complex structures. *Smart Materials and Structures* 16: 1489-1499.

Paget CA, Levin K and Delebarre C. (2002) Actuation performance of embedded piezoceramic transducer in mechanically loaded composites. *Smart Materials and Structures* 11: 886.

Pullin R, Eaton MJ, Pearson MR, et al. (2012) On the Development of a Damage Detection System using Macro-fibre Composite Sensors. *Journal of Physics: Conference Series* 382: 012049.

Salamone S, Bartoli I, Lanza Di Scalea F, et al. (2009) Guided-wave Health Monitoring of Aircraft Composite Panels under Changing Temperature. *Journal of Intelligent Material Systems and Structures* 20: 1079-1090.

Smart Material Corporation D, Germany.https://www.smart-material.com/MFC-product-P2.html Capacitance of MFC (model : M2814-P2) is 30.78 nF.

Sodano HA, Lloyd J and Inman DJ. (2006) An experimental comparison between several active composite actuators for power generation. *Smart Materials and Structures* 15: 1211-1216.

Sodano HA, Park G and Inman DJ. (2004) An investigation into the performance of macro-fiber composites for sensing and structural vibration applications. *Mechanical Systems and Signal Processing* 18: 683-697.

Song HJ, Choi Y-T, Wereley NM, et al. (2010) Energy Harvesting Devices Using Macro-fiber Composite Materials. *Journal of Intelligent Material Systems and Structures* 21: 647-658.

Tang HY, Winkelmann C, Lestari W, et al. (2011) Composite Structural Health Monitoring Through Use of Embedded PZT Sensors. *Journal of Intelligent Material Systems and Structures* 22: 739-755.
Weder A, Geller S, Heinig A, et al. (2013) A novel technology for the high-volume production of intelligent composite structures with integrated piezoceramic sensors and electronic components. *Sensors and Actuators A: Physical* 202: 106-110.
Yang SM, Hung CC and Chen KH. (2005) Design and fabrication of a smart layer module in composite laminated structures. *Smart Materials and Structures* 14: 315.
Zeng W, Zhou C, Xiao J and Ma J. (2015.) Correlation between temperature-dependent permittivity dispersion and depolarization behaviours in Zr^{4+}-modified $BiFeO_3$–$BaTiO_3$ piezoelectric ceramics. *Bulletin of Material Science* **38** 1737-1741